



## Data Article

# Data on the comprehensive first-principles diffusion study of the aluminum-magnesium system



M.S. Hooshmand, W. Zhong, J.C. Zhao, W. Windl, M. Ghazisaeidi\*

*Department of Materials Science and Engineering, Ohio State University, Columbus, OH 43210, USA*

## ARTICLE INFO

*Article history:*

Received 9 February 2020

Revised 25 February 2020

Accepted 26 February 2020

Available online 5 March 2020

*Keywords:*

Density functional theory (DFT)

Diffusion coefficients

Magnesium alloys

Aluminum alloys

Uncertainty analysis

## ABSTRACT

First-principles calculation of diffusion coefficients between Mg and Al is investigated comprehensively using density functional theory (DFT). The effect of different uncertainty sources arising from first principles calculations has been investigated systematically. These sources include the diffusion model, energetic, entropic and attempt frequency calculations. Variation in self and impurity diffusion coefficients of Mg and Al in stable phases are quantified using different DFT settings and compared with the experiments. Using the optimal DFT settings, diffusion coefficients in metastable phases of Al and Mg are predicted. The dataset refers to “An integrated experimental and computational study of diffusion and atomic mobility of the aluminum-magnesium system” [1].

© 2020 Published by Elsevier Inc.

This is an open access article under the CC BY-NC-ND license. (<http://creativecommons.org/licenses/by-nc-nd/4.0/>)

\* Corresponding author.

*E-mail addresses:* [hooshmand.1@osu.edu](mailto:hooshmand.1@osu.edu) (M.S. Hooshmand), [zhong.194@osu.edu](mailto:zhong.194@osu.edu) (W. Zhong), [jczhao@umd.edu](mailto:jczhao@umd.edu) (J.C. Zhao), [windl.1@osu.edu](mailto:windl.1@osu.edu) (W. Windl), [ghazisaeidi.1@osu.edu](mailto:ghazisaeidi.1@osu.edu) (M. Ghazisaeidi).

**Specification Table**

Subject area	Materials Science
Specific subject area	Aluminum-magnesium alloys
Type of data	Table Figure
How data were acquired	Systematic density functional theory calculations are performed to quantify the uncertainty sources of diffusivity predictions in Al-Mg system.
Data format	Raw Analyzed
Parameters for data collection	Calculated data were obtained using a plane-wave cutoff of 260 eV, a $6 \times 6 \times 6$ $k$ -point mesh for Brillouin zone integration with a Monkhorst-Pack grid and a first-order Methfessel-Paxton method with a smearing width of 0.2 eV for the electronic smearing.
Description of data collection	Data were calculated from atomistic simulations using Vienna Ab-initio Simulation Package (VASP) package.
Data source location	Columbus, OH, USA
Data accessibility	Repository name: Data in Brief Dataverse Direct URL to data: <a href="https://doi.org/10.7910/DVN/5IHKIC">https://doi.org/10.7910/DVN/5IHKIC</a> [2]
Related research article	Zhong et al. "An integrated experimental and computational study of diffusion and atomic mobility of the aluminum-magnesium system". <i>Acta Materialia</i> (2020) [1]

**Value of the Data**

- Systematic uncertainty analysis on the diffusivity prediction arising from the density functional theory (DFT) calculations is performed in magnesium-aluminum alloys. These calculations lead to the more accurate prediction of transport coefficients from first-principles atomistic simulations.
- Using the optimum DFT settings in predicting diffusion coefficients for the stable phases, self and impurity diffusion in the metastable phases, which cannot be assessed experimentally, can be evaluated from DFT calculations.
- The calculated diffusion data can be used to develop the fundamental mobility databases.

**1. Data description**

In this work, we calculate solute diffusion coefficients from the density functional theory (DFT) inputs by following the Green function solution to the master equation approach [3]. For impurity diffusion calculation in face-centered cubic (fcc) systems, we use five-frequency model [4]. Fig. 1 shows the five identical jumps representing the symmetrically unique vacancy/solute (solvent) jumps. These rates are defined as vacancy hops in the solvent ( $\omega_0$ ), vacancy rotation around the solute ( $\omega_1$ ), vacancy-solute exchange ( $\omega_2$ ), dissociation from ( $\omega_3$ ) and association towards ( $\omega_4$ ) the solute. Table 1 lists the attempt frequencies and migration barriers for the five frequencies for diffusion of Mg(Al) in fcc Al(Mg) along with the corresponding solute-vacancy binding energies.

To calculate the diffusion coefficients in hexagonal close packed (hcp) systems, we use sixteen-frequency model recently proposed by Agarwal and Trinkle [5]. Fig. 2 shows these symmetrically unique jumps in an hcp lattice following the notation in reference [5]. The symmetry-unique frequencies and solute/vacancy migration barriers are tabulated in Table 2 and Table 3.

For self-diffusion coefficients, the five-frequency model is reduced to one, vacancy jump to the nearest neighbor host atom. Similarly, sixteen-frequency jumps in hcp are reduced to two, vacancy jump to the nearest neighbor host atom on the basal and pyramidal planes. Table 4 lists the energy barriers and attempt frequencies for vacancy jumps in the elemental hcp and fcc systems.

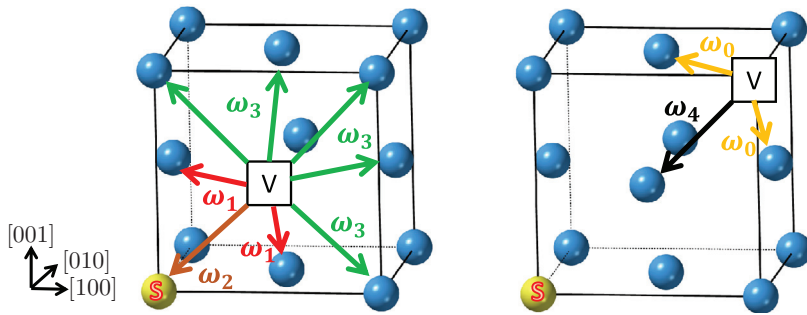


**Fig. 1.** Five-frequency jumps in fcc crystal structure. Solute (S) and vacancy (V) are indicated by yellow sphere and white square, respectively. Blue spheres represent host atom. (For interpretation of the references to color in this figure legend, the reader is referred to the web version of this article.)

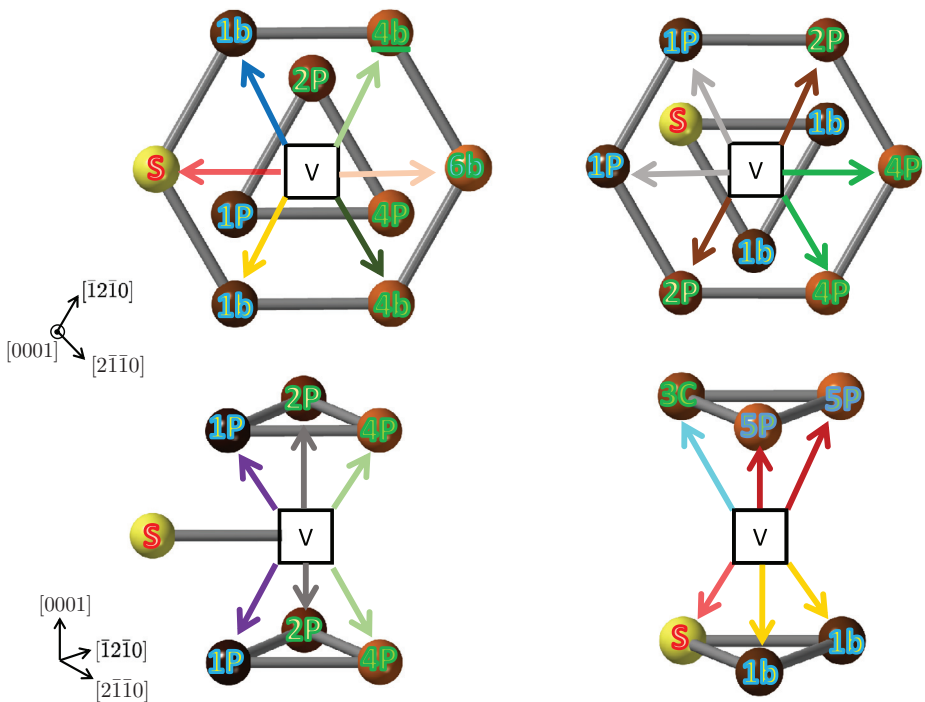


**Fig. 2.** Atomic hops considered in the diffusion model in hcp (based on the notations in [5]). Top and bottom rows show the basal and pyramidal jumps, respectively. Schematics in the left and right columns represent the solute and vacancy on the same plane (1b) and solute and vacancy on the different plane (1p), respectively. Note that the two reorientation jumps from 1b, that have been treated as a unique jump in previous models, are distinguished by 1b-1b in blue and  $\bar{1}b$ -1b in yellow in the top left figure. Solute (S) and vacancy (V) are indicated by yellow sphere and white square, respectively. Blue spheres represent host atom (modified after [5]). (For interpretation of the references to color in this figure legend, the reader is referred to the web version of this article.)

Vacancy formation energy and entropy are evaluated by calculating the Gibbs free energy of both the perfect supercell and the supercell with a vacancy at elevated temperature within the quasi-harmonic approximation (QHA) from phonon calculations [6]. Calculated vacancy formation energies and entropies are listed in Table 5. Finally, transition energies and attempt frequencies computed from DFT are used to compute the diffusion coefficients  $D$  and fitted into

**Table 1**

Migration barriers (eV) and attempt frequencies (THz) of jumps involved in the diffusion of Mg(Al) in fcc Al(Mg) within the five-frequency model [7]. Values calculated using ultra-soft pseudopotential (USPP) and the PBE functional are compared to the PAW with the PBEsol functional (PAW-PBEsol). Attempt frequencies from both density functional perturbation theory (DFPT) and finite difference method (FDM) using PAW-PBEsol functional are calculated and compared. Solute-vacancy nearest-neighbor binding energies are also listed.

System	Quantity	DFT Settings	Binding Energy (eV)	Solvent Diffusion	Rotation	Exchange	Dissociation	Association
				$\omega_0$	$\omega_1$	$\omega_2$	$\omega_3$	$\omega_4$
Mg in fcc Al	$E^{mig}(eV)$	USPP	0.008	0.537	0.680	0.393	0.477	0.457
		PAW-PBEsol	-0.006	0.707	0.744	0.465	0.590	0.663
	$\nu(THz)$	DFPT	-	6.475	9.309	43.783	10.264	6.064
		FDM	-	14.814	3.152	4.832	8.842	18.128
Al in fcc Mg	$E^{mig}(eV)$	USPP	-0.01	0.361	0.284	0.541	0.410	0.407
		PAW-PBEsol	-0.038	0.378	0.317	0.611	0.365	0.444
	$\nu(THz)$	DFPT	-	11.875	6.356	9.605	8.011	14.791
		FDM	-	16.879	33.407	57.861	338.230	20.771

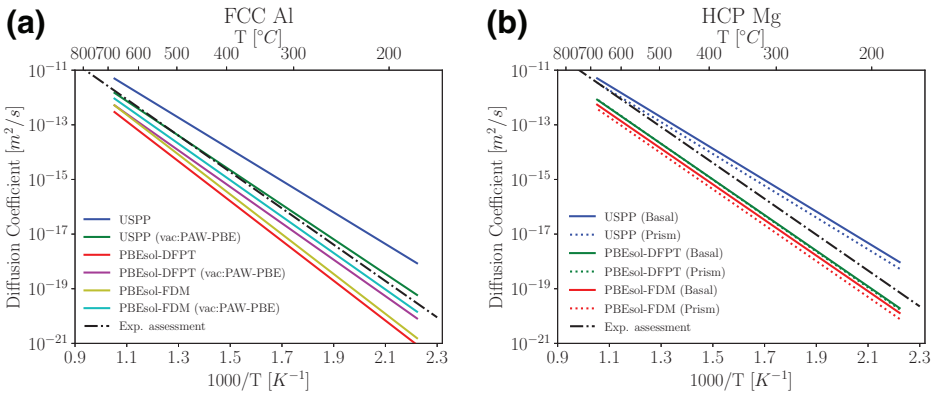


**Fig. 3.** Self diffusion coefficients for fcc Al and hcp Mg. DFT-derived values using different exchange-correlation pseudopotentials and attempt frequency calculation methods are compared with the experimental assessment in reference [1]. For Al systems, diffusivity values with the vacancy formation energy and entropy evaluated from regular PAW-PBE is also shown.

the conventional Arrhenius form:

$$D = D_0 \exp\left(-\frac{E_{act}}{k_B T}\right) \tag{1}$$

where  $D_0$  and  $E_{act}$  are diffusion prefactor and activation energy for diffusion, respectively.

Fig. 3 shows the calculated self-diffusion in fcc Al and hcp Mg using different exchange correlation (XC) functionals of ultra-soft pseudopotential (USPP) and projector augmented wave (PAW) compared with the experimental assessment done by Zhong et al.[1]. According to the Arrhenius equation in Equation 1, the slope of the calculated diffusivity lines corresponds to the activation energy  $E_{act}$  and the intercept with vertical axis corresponds to the diffusion pre-factor  $D_0$ . While the migration energies and vacancy formation energies mainly contribute to the  $E_{act}$ , vacancy formation entropy and migration frequencies mainly influence  $D_0$ . Table 6 lists the Arrhenius fit to the self-diffusivities using different DFT settings and compares those with some previous studies reported in the literature. Self diffusion coefficient data points at each temperature can be found in reference [2].

Fig. 4 shows the calculated Mg/Al impurity diffusion in fcc Al/hcp Mg. Table 7 lists the Arrhenius fit to the calculated diffusivities for impurity diffusion coefficients and compares these

**Table 2**

Migration barriers (eV) and attempt frequencies (THz) for the diffusion of dilute Mg(Al) in hcp Al(Mg) from the 1b configuration following the notation in reference [5]. Migration barriers from previous DFT works are also included for comparison (cf. Fig. 2 for notation and the caption in Table 1 for DFT settings interpretation).

System	Quantity	DFT Settings	Binding Energy(eV)	Exchange 1b-sol	Reorientation			Dissociation				
					1b-1b	1b-1b	1b-1p	1b-2p	1b-4p	1b-4b	1b-4b	1b-6b
Al in hcp Mg	$E^{\text{mig}}$ (eV)	USPP	-0.039	0.511	0.225	0.366	0.303	0.458	0.407	0.407	0.383	0.382
		PAW-PBEsol	-0.046	0.554	0.251	0.388	0.326	0.481	0.431	0.432	0.408	0.406
		Ref. [5]	-0.027	0.524	0.240	0.378	0.318	0.472	0.426	0.424	0.399	0.392
	$\nu$ (THz)	Ref. [8]	-	0.599	-	0.372	0.343	-	-	-	-	0.414
		DFPT	-	39.943	7.313	7.628	8.686	11.892	10.915	8.436	9.346	8.566
		FDM	-	7.369	4.419	10.442	4.043	4.201	2.552	8.909	2.469	3.660
Mg in hcp Al	$E^{\text{mig}}$ (eV)	USPP	-0.013	0.305	0.621	0.452	0.541	0.385	0.403	0.363	0.409	0.381
		PAW-PBEsol	-0.069	0.432	0.768	0.597	0.696	0.537	0.555	0.516	0.551	0.528
	$\nu$ (THz)	DFPT	-	14.842	6.471	14.070	25.784	5.223	9.475	11.204	3.294	2.952
		FDM	-	16.165	9.229	13.131	32.697	6.023	11.974	13.225	3.813	3.257

**Table 3**

Migration barriers (eV) and attempt frequencies (THz) for the diffusion of dilute Mg(Al) in hcp Al(Mg) from the 1p configuration following the notation in reference [5]. Migration barriers from previous DFT works are also included for comparison (cf. Fig. 2 for notation and the caption in Table 1 for DFT settings interpretation).

System	Quantity	DFT Settings	Binding Energy(eV)	Exchange	Reorientation		Dissociation			
				1p-sol	1p-1p	1p-1b	1p-2p	1p-3c	1p-4p	1p-5p
Al in hcp Mg	$E^{\text{mig}}$ (eV)	USPP	-0.031	0.546	0.292	0.295	0.428	0.447	0.391	0.395
		PAW-PBEsol	-0.041	0.595	0.333	0.319	0.451	0.492	0.418	0.435
		Ref. [5]	-0.020	0.567	0.308	0.311	0.441	0.471	0.409	0.414
	$\nu$ (THz)	Ref. [8]	-	0.654	0.326	0.326	-	-	0.418	-
		DFPT	-	52.310	81.356	9.771	13.030	9.341	10.072	187.880
		FDM	-	7.388	13.725	2.818	3.706	4.271	4.663	12.181
Mg in hcp Al	$E^{\text{mig}}$ (eV)	USPP	-0.019	0.294	0.514	0.545	0.370	0.376	0.399	0.420
		PAW-PBEsol	-0.074	0.423	0.667	0.702	0.522	0.523	0.546	0.590
	$\nu$ (THz)	DFPT	-	19.994	11.461	16.976	3.820	8.438	7.847	19.901
		FDM	-	19.316	10.836	21.210	3.525	8.665	6.032	19.747

**Table 4**

Migration energies (eV) and attempt frequencies (THz) for vacancy mediated diffusion in elemental fcc/hcp Al and Mg. For hcp systems, the values for basal and (pyramidal) jumps are shown without and (with) parentheses. For DFT settings tags interpretation, refer to the caption in the text and Table 1.

Quantity	DFT Settings	hcp Mg	fcc Al	fcc Mg	hcp Al
$E^{\text{mig}}$ (eV)	USPP	0.383 (0.402)	0.565	0.398	0.423 (0.448)
	PAW-PBEsol	0.407 (0.423)	0.633	0.363	0.502 (0.523)
$\nu$ (THz)	DFPT	5.018 (6.497)	4.854	7.715	7.844 (7.553)
	FDM	3.873 (2.759)	6.958	8.742	9.712 (4.883)

**Table 5**

Vacancy formation energies and vacancy formation entropies in fcc/hcp Al/Mg systems using different DFT settings. For Al cells, calculated values from regular PAW-PBE functional are also reported.

System	DFT Settings	$H_V^f$ (eV)	$S_V^f$ ( $k_B$ )
hcp Mg	USPP	0.755	1.591
	PAW-PBEsol	0.883	1.968
fcc Al	USPP	0.582	1.277
	PAW-PBE	0.690	1.393
fcc Mg	PAW-PBEsol	0.813	2.324
	USPP	0.580	0.313
hcp Al	PAW-PBEsol	0.893	1.716
	USPP	0.509	0.371
	PAW-PBE	0.690	1.393
	PAW-PBEsol	0.710	1.031

**Table 6**

Arrhenius fit to the calculated self-diffusion coefficients. Diffusivities are fit to the  $D = D_0 \exp(-E_{act}/k_B T)$  equation, where  $D$ ,  $D_0$ , and  $E_{act}$  are diffusivity, diffusion prefactor and activation energy barrier, respectively. These values are compared to the experimental values reported in the literature. For Al systems, fit to the diffusivity data derived from regular PAW-PBE functional for vacancy formation energies and entropies are also included. For hcp systems, diffusivity values for basal and ( $\bar{c}$ ) are shown without and (with) parentheses. For DFT settings tags interpretation, refer to the caption in the text and Table 1.

System	DFT Settings	$D_0$ ( $m^2/s$ )	$E_{act}$ (eV)
hcp Mg	USPP	5.76E-06 (4.62E-06)	1.14 (1.15)
	PAW-PBEsol, DFPT	6.15E-06 (7.17E-06)	1.29 (1.30)
	PAW-PBEsol, FDM	3.99E-06 (3.21E-06)	1.29 (1.30)
	Assessed experimental data [1]	2.88E-05	1.30
fcc Al	Ref. [9] (Experimental)	2.00E-04 (2.03E-03)	1.44 (1.46)
	USPP	5.98E-06	1.15
	USPP(vac:PAW-PBE)	6.71E-06	1.25
	PAW-PBEsol, DFPT	1.38E-05	1.45
	PAW-PBEsol, DFPT (vac:PAW-PBE)	5.42E-06	1.32
	PAW-PBEsol, FDM	2.42E-05	1.45
	PAW-PBEsol, FDM (vac:PAW-PBE)	9.55E-06	1.32
fcc Mg	Assessed experimental data [1]	1.79E-05	1.32
	PAW-PBEsol, FDM	1.49E-05	1.26
hcp Al	PAW-PBEsol, FDM	2.87E-06 (1.92E-06)	1.22 (1.23)
	PAW-PBEsol, FDM (vac:PAW-PBE)	4.11E-06 (2.76E-06)	1.20 (1.21)

values with the experimental assessment reported in [1]. All the raw diffusion values are also provided in the Data in Brief Dataverse [2].

Based on these findings, we predict the diffusion coefficients in metastable (hypothetical) phases using optimum DFT settings in the stable phases. Elemental self-diffusivities in hcp Al

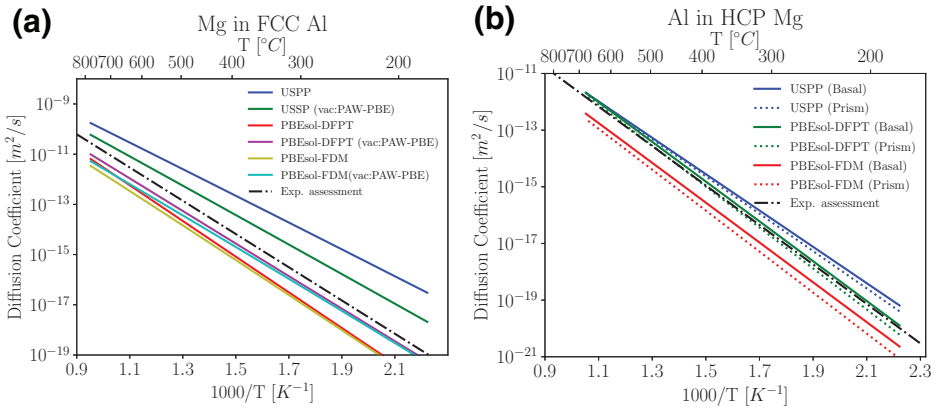


**Fig. 4.** Impurity diffusion coefficients: (a) Mg in fcc Al and (b) Al in hcp Mg. DFT-derived values using different exchange-correlation pseudopotentials and attempt frequency calculation methods are compared with the experimental assessment in reference [1]. For Al systems, diffusivity values with the vacancy formation energy and entropy evaluated from regular PAW-PBE is also shown.

**Table 7**

Arrhenius fit to the calculated impurity diffusion coefficients. Diffusivities are fit to the  $D = D_0 \exp(-E_{act}/k_B T)$  equation, where  $D$ ,  $D_0$ , and  $E_{act}$  are diffusivity, diffusion prefactor and activation energy barrier, respectively. These values are compared to the experimental values reported in the literature. For Al systems, fit to the diffusivity data where the regular PAW-PBE functional is used to calculate vacancy formation energies and entropies are also included. For hcp systems, diffusivity values for basal and  $\bar{c}$  are shown without and (with) parentheses. For DFT settings tags interpretation, refer to the caption in the text and Table 1.

System	DFT Settings	$D_0$ (m <sup>2</sup> /s)	$E_{act}$ (eV)
Al in hcp Mg	USPP	1.17E-05 (1.78E-05)	1.27 (1.31)
	PAW-PBEsol, DFPT	5.12E-05 (7.09E-05)	1.39 (1.43)
	PAW-PBEsol, FDM	9.52E-06 (1.00E-05)	1.39 (1.43)
	Assessed experimental data [1]	3.13E-05	1.38
	Ref. [5] (DFT)	1.87E-06 (2.02E-06)	1.46
	Ref. [10] (DFT)	3.44E-05 (3.11E-5)	1.41
	Ref. [8] (DFT)	4.24E-06 (7.17E-06)	1.29
Mg in fcc Al	USPP	2.06E-05	1.06
	USPP(vac:PAW-PBE)	2.30E-05	1.16
	PAW-PBEsol, DFPT	3.72E-05	1.41
	PAW-PBEsol, DFPT (vac:PAW-PBE)	1.47E-05	1.29
	PAW-PBEsol, FDM	1.45E-05	1.38
	PAW-PBEsol, FDM (vac:PAW-PBE)	5.70E-06	1.25
	Assessed experimental data [1]	5.61E-05	1.31
Al in fcc Mg	PAW-PBEsol, DFPT	1.03E-05	1.46
Mg in hcp Al	PAW-PBEsol, DFPT	8.58E-06 (1.08E-05)	1.19 (1.20)
	PAW-PBEsol, DFPT (vac:PAW-PBE)	5.04E-06 (6.31E-05)	1.08 (1.10)

and fcc Mg, and Al/Mg impurity diffusion in fcc Mg/hcp Al are shown in Fig. 5 and the Arrhenius fit is listed in Tables 6 and 7.

**2. Experimental design, materials, and methods**

An integration of diffusion multiples and forward-simulation analysis was employed to experimentally investigate the diffusion between polycrystalline Al (99.95 wt.%) and Mg (99.95 wt.%) at four temperatures between 275°C and 420°C [1]. The interdiffusion coefficients in the stable

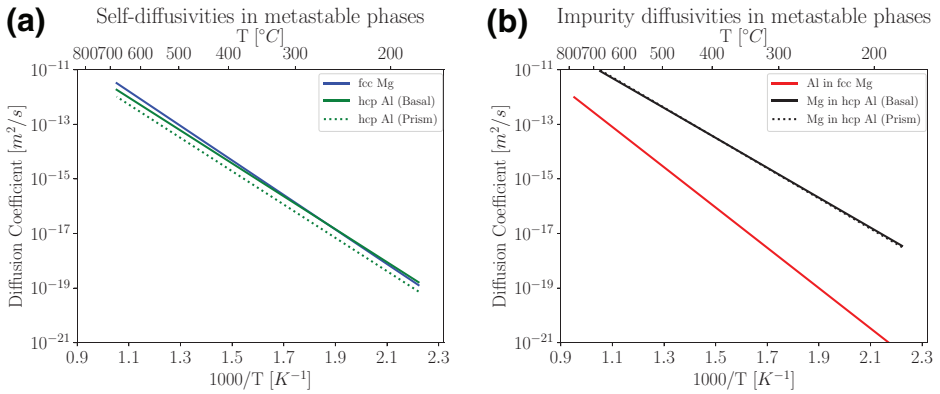


**Fig. 5.** Diffusion coefficients in metastable phases: (a) self-diffusivities in elemental hcp Al and fcc Mg, (b) impurity diffusion of Al in fcc Mg and Mg in hcp Al using the optimized DFT settings identified for stable phases as explained in the text.

phases fcc Al, hcp Mg,  $\beta$  –  $\text{Mg}_{17}\text{Al}_{12}$ ,  $\gamma$  –  $\text{Mg}_2\text{Al}_3$ ,  $\varepsilon$  –  $\text{Mg}_{23}\text{Al}_{30}$  as well as the impurity diffusion coefficients in fcc Al and hcp Mg were extracted. The design of the diffusion multiples and the experimental procedure were described concretely in the Section 2.1 of reference [1]. The experimental diffusion coefficients of the Al-Mg system in the literature were also collected (cf. Tables 1–3 in reference [1]) to assess the self-diffusion coefficients of fcc Al/hcp Mg and impurity diffusion coefficients of Al/Mg in hcp Mg/fcc Al along with the data obtained from this work. The best judgements of those four dilute diffusion coefficients in the stable fcc Al and hcp Mg phases serve as the criteria to evaluate the result quality of DFT calculations to identify the optimal settings to compute the dilute diffusion coefficients of Al and Mg in metastable phases (hcp Al and fcc Mg).

DFT calculations are performed using VASP package [11], a plane-waved based density functional code. We compare ultra-soft pseudopotential (USPP) [12] with projector augmented wave (PAW) [13] formalism based potentials within the generalized gradient approximation (GGA) exchange correlation. In particular, we implement Perdew-Burke-Ernzerhof [14] (labeled as PBE) and a modified version by incorporating surface energy error correction [15] (labeled as PBEsol) functionals. A plane-wave cutoff of 260 eV is used throughout the calculations. A  $4 \times 4 \times 3$  (96 atoms) and a  $3 \times 3 \times 3$  (108 atoms) supercell is employed for hcp and fcc structures, respectively. For electronic smearing, the first-order Methfessel-Paxton method [16] with a smearing width of 0.2 eV is used. A  $6 \times 6 \times 6$   $k$ -point mesh is used for Brillouin zone integration with a Monkhorst-Pack grid for all supercells.  $\Gamma$ -point is included in the  $k$ -mesh for hcp systems. Conjugate gradient method is used for minimizing the energy of all atoms until the forces are less than 0.1 meV/Å. The calculated lattice parameters using the settings above are  $a = 4.04$  Å for fcc-Al,  $a = 4.51$  Å for fcc-Mg,  $a = 3.69$  Å;  $\frac{c}{a} = 1.41$  for hcp Mg and  $a = 3.29$  Å;  $\frac{c}{a} = 1.44$  for hcp Al. Vacancy hop rate follows  $\omega = \nu_0 \exp(-E_a/k_B T)$ , where  $\nu_0$  is the attempt frequency and  $E_a$  the energy difference between saddle point and initial configuration, assuming transition state theory.  $k_B$  and  $T$  are Boltzmann constant and temperature, respectively.

To calculate the transition state configuration and energy, we use climbing-image nudged elastic band (CI-NEB) method with one intermediate image [17]. These CI-NEB calculations are continued until the forces are converged to within 5 meV/Å. Attempt frequency associated with each transition,  $\nu$ , in a supercell with  $N$  number of atoms is computed from Vineyard's equation:

$$\nu = \frac{\prod_{k=1}^{3N} \nu_k}{\prod_{k=1}^{3N-1} \nu'_k} \quad (2)$$

where  $\nu_k$  and  $\nu'_k$  are the real normal mode frequencies at the local energy minimum and saddle point configuration, respectively. We implement and compare finite difference method (FDM) [18] and density functional perturbation theory (DFPT) [19] approaches to calculate the restoring forces and derive the Hessian matrix. Individual phonon frequencies are the square root of the eigenvalues of the Hessian matrix. To evaluate the vacancy formation energy and entropy, we calculate the vibrational contribution to the free energy of both perfect and vacancy cells using the Phonopy package [20].

## Acknowledgment

This work is supported by the U.S. Department of Energy, Office of Science, Basic Energy Sciences, under Award # DE-SC0012481. This work also acknowledges funding by the Center for Performance and Design of Nuclear Waste Forms and Containers, an Energy Frontier Research Center funded by the U.S. Department of Energy, Office of Science, Basic Energy Sciences under Award # DE-SC0016584. Computational resources were provided through the Ohio Supercomputer Center.

## Conflict of Interest

The authors declare that they have no known competing financial interests or personal relationships that could have appeared to influence the work reported in this paper.

## References

- [1] W. Zhong, M.S. Hooshmand, M. Ghazisaeidi, W. Windl, J.C. Zhao, An integrated experimental and computational study of diffusion and atomic mobility of the aluminum-magnesium system, *Acta Mater.* (2020), doi:10.1016/j.actamat.2019.12.054.
- [2] M.S. Hooshmand, First-principles self and impurity diffusion data of the Al-Mg system, Harvard Dataverse, V1, 2020. doi:10.7910/DVN/5IHKIC.
- [3] D.R. Trinkle, Automatic numerical evaluation of vacancy-mediated transport for arbitrary crystals: Onsager coefficients in the dilute limit using a green function approach, *Philos. Mag.* 97 (28) (2017) 2514–2563.
- [4] A.L. Claire, Solute diffusion in dilute alloys, *J. Nucl. Mater.* 69 (1978) 70–96.
- [5] R. Agarwal, D.R. Trinkle, Exact model of vacancy-mediated solute transport in magnesium, *Phys. Rev. Lett.* 118 (10) (2017) 105901.
- [6] S.-L. Shang, Y. Wang, D. Kim, Z.K. Liu, First-principles thermodynamics from phonon and Debye model: application to Ni and Ni<sub>3</sub>Al, *Comput. Mater. Sci.* 47 (4) (2010) 1040–1048.
- [7] H. Mehrer, *Diffusion in Solids: Fundamentals, Methods, Materials, Diffusion-Controlled Processes*, 155, Business Media, 2007.
- [8] S. Ganeshan, L. Hector Jr., Z.K. Liu, First-principles calculations of impurity diffusion coefficients in dilute Mg alloys using the 8-frequency model, *Acta Mater.* 59 (8) (2011) 3214–3228.
- [9] J. Combronde, G. Brebec, Anisotropie d'autodiffusion du magnésium, *Acta Metall.* 19 (12) (1971) 1393–1399.
- [10] B.-C. Zhou, S.-L. Shang, Y. Wang, Z.K. Liu, Data set for diffusion coefficients of alloying elements in dilute Mg alloys from first-principles, *Data Brief* 5 (2015) 900–912.
- [11] G. Kresse, J. Furthmüller, Efficient iterative schemes for ab initio total-energy calculations using a plane-wave basis set, *Phys. Rev. B* 54 (16) (1996) 11169–11186.
- [12] D. Vanderbilt, Soft self-consistent pseudopotentials in a generalized eigenvalue formalism, *Phys. Rev. B* 41 (11) (1990) 7892.
- [13] P.E. Blöchl, Projector augmented-wave method, *Phys. Rev. B* 50 (24) (1994) 17953.
- [14] J.P. Perdew, K. Burke, M. Ernzerhof, Generalized gradient approximation made simple, *Phys. Rev. Lett.* 77 (18) (1996) 3865.
- [15] J.P. Perdew, A. Ruzsinszky, G.I. Csonka, O.A. Vydrov, G.E. Scuseria, L.A. Constantin, X. Zhou, K. Burke, Restoring the density-gradient expansion for exchange in solids and surfaces, *Phys. Rev. Lett.* 100 (13) (2008) 136406.
- [16] M. Methfessel, A. Paxton, High-precision sampling for Brillouin-zone integration in metals, *Phys. Rev. B* 40 (6) (1989) 3616.
- [17] G. Henkelman, B.P. Uberuaga, H. Jónsson, A climbing image nudged elastic band method for finding saddle points and minimum energy paths, *J. Chem. Phys.* 113 (22) (2000) 9901–9904.
- [18] G. Kresse, J. Furthmüller, J. Hafner, Ab initio force constant approach to phonon dispersion relations of diamond and graphite, *EPL (Europhys. Lett.)* 32 (9) (1995) 729.
- [19] G.P. Srivastava, *The Physics of Phonons*, CRC Press, 1990.
- [20] A. Togo, I. Tanaka, First principles phonon calculations in materials science, *Scr. Mater.* 108 (2015) 1–5.